A marine carbon monoxide (CO) model with a new parameterization of microbial oxidation

Young Shin Kwon[a,b], Hyoun-Woo Kang[c,*], Luca Polimene[d], Tae Siek Rhee[a]

[a] Korea Polar Research Institute, Incheon, Korea
[b] University of Science and Technology, Daejeon, Korea
[c] Korea Institute of Ocean Science and Technology, Busan, Korea
[d] Plymouth Marine Laboratory, Plymouth, U.K

ARTICLE INFO

ABSTRACT

Traditionally, marine carbon monoxide (CO) models assume that the microbial oxidation of CO is only dependent on the concentration of CO in the water column. However, CO oxidation rates in the ocean have been reported to vary up to two orders of magnitude both spatially and temporally. Here, we developed a new model assuming that CO microbial oxidation is dependent on bacterial carbon biomass other than CO concentration. In addition to microbial oxidation, the model also describes CO photochemical production, vertical mixing, and air-sea gas exchange. The new CO model has been embedded in the European Regional Seas Ecosystem Model (ERSEM) and coupled with the General Ocean Turbulence Model (GOTM). The CO-GOTM-ERSEM model was implemented at the Bermuda Atlantic Time Series (BATS) station to simulate CO concentrations observed in March 1993 by Kettle (1994). The proposed second-order function describing CO microbial oxidation introduces a new parameter, the bacteria biomass specific oxidation rate, which was estimated to be 5.7 ± 0.2 (μg C m^{-3})$^{-1}$ h^{-1}. Statistical metrics indicates that the new CO model performs better than a previously published model with a first-order decay function to describe microbial oxidation, acknowledging the dependence of microbial oxidation on bacterial abundance is realistic. A long-term (1992 - 1994) simulation carried out with CO-GOTM-ERSEM reproduced the spatial and seasonal variability of CO reported in the literature. Our model provides a realistic description of the CO dynamics and is potentially usable in different environmental contexts worldwide.

1. Introduction

Carbon monoxide (CO) plays two key roles in the atmosphere: 1) it impacts on climate forcing by competing with the methane in the reaction with the hydroxyl radical (Daniel and Solomon, 1998), the main atmospheric oxidant, and 2) it is involved in the production of ozone (Logan et al., 1981), which in turn leads to the photochemical smog, reducing atmospheric visibility. Therefore, considering its impact on the chemical properties of the atmosphere, CO is regarded as one of the most important trace gasses (Stocker et al., 2013).

Although most of the atmospheric CO is emitted from the continent, outgassing from the sea surface could be a significant source in the remote marine environments and in the southern hemisphere where the CO in the surface ocean is supersaturated with respect to the overlying air (Bates et al., 1995; Conrad et al., 1982; Khalil and Rasmussen, 1990; Logan et al., 1981; Rhee, 2000; Stubbins et al., 2006; Zafiriou et al., 2003). Understanding CO dynamics in the marine upper layer is thereby crucial to assess the role played by this gas in the global climate regulation.

The concentration of dissolved CO in the surface ocean results from the balance between photochemical production (Conrad et al., 1982; Redden, 1982; Zuo and Jones, 1995), microbial oxidation (Conrad et al., 1982; Jones and Amador, 1993; Jones and Morita, 1984), air-sea gas exchange (Bates et al., 1995; Conrad et al., 1982; Park and Rhee, 2016; Zuo and Jones, 1995), and vertical mixing (Doney et al., 1995; Gnanadesikan, 1996; Johnson and Bates, 1996; Kettle, 1994) (Fig. 1). Among these processes, photochemical production and microbial oxidation are the major processes contributing to the CO budget in the ocean (Zafiriou et al., 2003). Indeed, photolysis of chromophoric dissolved organic matter (CDOM) in the euphotic zone is the only known source of CO, while microbial oxidation is by far the dominant sink, destroying more than 80% of the CO pool. Therefore, an accurate parameterization of microbial oxidation is essential to estimate CO flux from the upper ocean (Moran and Miller, 2007). Microbial
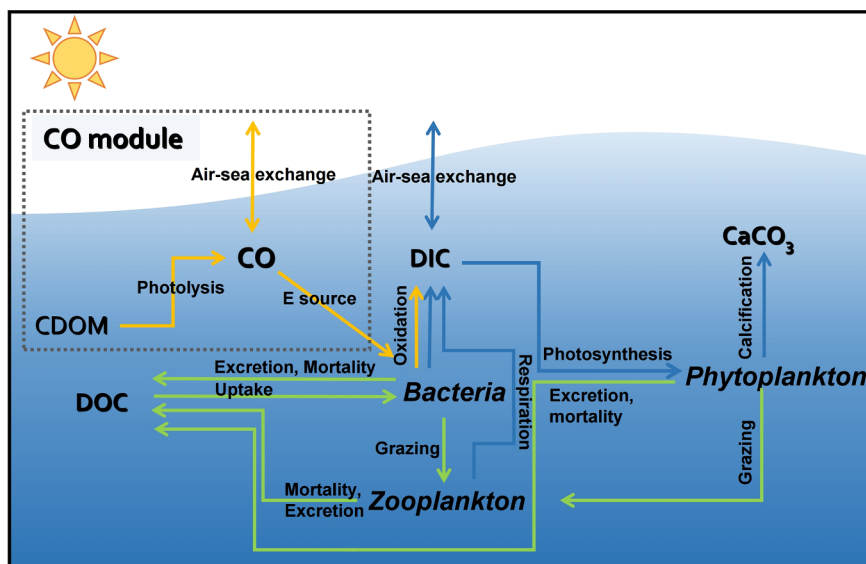
Fig. 1. Schematic diagram of marine carbon cycle (green and blue arrows for organic and inorganic species, respectively) and CO dynamics (yellow arrows) in the surface mixed layer. The model developed in this study for CO dynamics was incorporated in the carbon cycle using a complex ecosystem model. (For interpretation of the references to colour in this figure legend, the reader is referred to the web version of this article.)

CO oxidation is described conventionally as a first-order kinetics (Conrad et al., 1982; Johnson and Bates, 1996; Jones, 1991; Jones and Amador, 1993; Xie et al., 2005; Zafiriou et al., 2003), assuming that CO oxidation rate increases linearly with the increase of dissolved CO concentrations, regardless of microbial abundance and community composition.

Several modeling studies of marine CO dynamics were carried out to understand the CO budget in the ocean. Kettle (1994) developed a model to understand the surface diurnal pattern of dissolved CO concentrations at the Bermuda Atlantic Time-series Study (BATS) station in the Sargasso Sea. The model adopted the Price-Weller-Pinkel (PWP) vertical mixing scheme (Price et al., 1986) to simulate the physical mixing and transport in the surface mixed layer and subsurface layers. CO production was simulated by using a modified version of the photochemical production module previously developed for dissolved hydrogen peroxide (H_2O_2) in the marine environments by Sikorski and Zika (1993). In subsequent studies (Kettle, 2000, 2005b), an optimization technique was used to reduce the discrepancy between observed and simulated dissolved CO concentrations. Based on the CO observation by Kettle (1994), Gnanadesikan (1996) developed a simple model coupling CO dynamics with a bulk mixed layer model to identify nine marine regimes corresponding to different interactions between physical mixing and (photochemical) productions. The regimes were defined depending on the ratios between physical length scales, i.e. the depths to which vertical mixing, ventilation, and photochemically active radiation penetration occur. The critical difference between the models of Gnanadesikan (1996) and Kettle (1994) is the way they describe CO photochemical production: while Kettle (1994) considered the variation of CO photoproduction rate depending on the spectral irradiance, Gnanadesikan (1996) assumed that the photoproduction is proportional to a fraction of the total irradiance.

Simple box models were also used to determine the ratio between photochemical production and microbial oxidation (Johnson and Bates, 1996; Kitidis et al., 2011). Johnson and Bates (1996) determined the photoproduction and oxidation rates using the exponential fits of their observed diurnal variations of CO. Kitidis et al. (2011) took the production and oxidation rates from their experimental measurements and considered the vertical gradient of CO concentration due mainly to the light attenuation with depth.

All the above mentioned modeling studies used a first-order kinetics to describe CO microbial oxidation implicitly assuming that the CO microbial oxidation rate is constant in the ocean. However, this assumption is not consistent with experimental studies reporting that the CO oxidation rates (k_{CO}) varies dramatically (0.003 - 1.11 h^{-1}) both

temporally and spatially (Johnson and Bates, 1996; Jones, 1991; Jones and Amador, 1993; Kwon, 2015; Xie et al., 2005). Moreover, Xie et al. (2005, 2009) reported complex influences of various biotic and abiotic variables on this process showing that k_{CO} is dependent on temperature, primary production and salinity. These studies suggest that previously used formulations can only be reliable in specific conditions (i.e. specific location and time of the year), but cannot be used in modeling work dealing with large spatial (e.g. global models) and temporal scales (from seasonal upward).

The aim of this paper is to provide a novel model formulation able to simulate the variability of CO oxidation rate described in literature. To this end, we tested the hypothesis that microbial CO oxidation is a function of not only dissolved CO concentration but also bacterial biomass. Our CO model was implemented in a widely used marine ecosystem model, the European Regional Seas Ecosystem Model (ERSEM; Butenschön et al., 2016). Since ERSEM only accounts for heterotrophic bacteria, we assumed that the activity of CO oxidizing bacteria is proportional to the biomass of the heterotrophic bacteria community. This assumption is supported by the several studies (Gonzalez and Moran, 1997; Gonzalez et al., 2000; Moran et al., 2004; Suzuki et al., 2001; Tolli et al., 2006) which show that CO oxidizing bacteria (*Roseobacter*-associated clade) are ubiquitous in the ocean and that account for a relatively constant fraction of the heterotrophic bacterial biomass.

2. Methods

2.1. CO model with a new formulation of microbial oxidation

Temporal and spatial variability of dissolved CO concentrations ([CO]) in the water column was formulated as a function of depth (z) and time (t) associated with photochemical production (J), air-sea gas exchange ($F, z = 0$), vertical mixing (V), and microbial oxidation (M):

$$\frac{d[CO]}{dt} = J(z, t) + F(0, t) + V(z, t) + M(z, t) \tag{1}$$

The detailed formulation of the four processes on the right hand side of Eq. (1) are described in the following sections.

2.1.1. Photochemical production (J)

Photolysis rate of gas species in the atmosphere is determined by the actinic flux of the sun, absorption property of a reactant, and the quantum yield representing the production efficiency. Analogous mechanisms have been applied to the photochemical production of the CO

in the ocean taking into account the attenuation of the irradiance in the water column (Kettle, 1994; Zafiriou et al., 1984):

$$J(z, t) = \int_{\lambda_1}^{\lambda_2} E(\lambda, z, t) \ a_g(\lambda)\Phi(\lambda) \ d\lambda \tag{2}$$

where $E(\lambda, z, t)$ indicates solar spectral irradiance at the given wavelength (λ), depth (z), and time (t). $a_g(\lambda)$ and $\Phi(\lambda)$ indicate the absorption coefficient of CDOM and the apparent quantum yield of CO at the given wavelength, respectively. In this study, 280 and 800 nm were adopted as λ_1 and λ_2, respectively, as most of CO production occurs at the wavelength shorter than the visible wavelengths (Kettle, 1994; Valentine and Zepp, 1993).

$E(\lambda, z, t)$ can be replaced by a fraction of the total surface irradiance, $E_T(z, t)$. Therefore the right hand side of Eq. (2) becomes:

$$J(z, t) = 0.51 \ E_T(z, t) \int_{280}^{800} a_g(\lambda) \ \Phi(\lambda) \ d\lambda \tag{3}$$

where 0.51 is the solar irradiance penetrating the water surface and consists of 42% of visible light and 9% of ultraviolet (UV) light on average (Gibson, 2003).

$a_g(\lambda)$ can also be described as an exponential decrease of $a_g(\lambda_0)$ with slope S, where $a_g(\lambda_0)$ is a reference absorption coefficient at λ_0 (Bricaud et al., 1995, 1981; Green and Blough, 1994):

$$a_g(\lambda) = a_g(\lambda_0) \ e^{-S(\lambda - \lambda_0)} \tag{4}$$

While several experiments conducted in the coastal area (Anderson and Stedmon, 2007; Asmala et al., 2012; Coble, 2007; Ferrari, 2000; Ferrari et al., 1996; Mannino et al., 2008; Rochelle-Newall and Fisher, 2002; Stedmon et al., 2000; Vodacek et al., 1997) showed a linear relationship between dissolved organic carbon concentrations ([DOC]) and the absorption coefficient of CDOM at a specific wavelength, $a_g(\lambda_0)$, Nelson et al. (1998) and Nelson and Siegel (2013) found no relationship in the open ocean and in the Sargasso Sea (Siegel et al., 2002) at Bermuda from 1996 to 1999. Thereby, regardless of [DOC], we assumed $a_g(\lambda_0)$ to be constant at the value of 0.2 m^{-1} as determined by Kettle (1994) in the same area by using a reference wavelength of 300 nm (λ_0) and the reference slope (S) of -0.020 nm^{-1} (Kettle, 2005b; Kitidis et al., 2011).

We adopted the exponential fitting curve of $\Phi(\lambda)$ developed by Kettle (2005b) based on experimental results at BATS (Kettle, 1994):

$$\Phi(\lambda) = 2.427e^{-0.0302\lambda} \tag{5}$$

2.1.2. Air-sea flux (F)

The air-sea CO flux was calculated by a mass transfer equation as follows:

$$F(0, t) = k_w \ ([CO](0, t) - L \ pCO) \tag{6}$$

where k_w is the gas transfer velocity of CO, $[CO](0, t)$ and pCO are the concentration of CO at the sea surface at the given time and partial pressure of CO in the overlying air, respectively, and L is the solubility of CO (Wiesenburg and Guinasso, 1979).

We assumed that the CO is homogeneously distributed in the upper layer in the model. Previous findings support our assumption that dissolved CO concentration is virtually constant in the first 5 m during the day (Johnson, 1999). pCO was calculated as a product of the mole fraction of atmospheric CO and the atmospheric pressure at BATS assuming that water vapor was saturated. The mean CO mole fraction (169 ppb) observed in March 1993 by the atmospheric monitoring station, BMW (Bermuda West), run by NOAA/ESRL (National Oceanic and Atmospheric Administration/Earth System Research Laboratory; https://www.esrl.noaa.gov/gmd/dv/data/), was used for our calculation.

k_w was parameterized following Nightingale et al. (2000) because it

is indifferent from the recently suggested parameterizations (Ho et al., 2011; Wanninkhof, 2014) implying its reliability, and it has already been used to model air-sea CO_2 and O_2 exchange with ERSEM (Butenschön et al., 2016). Accounting for the change in diffusivities of both CO and momentum at different thermodynamic conditions of the seawater from the reference condition (Temperature = 20 °C and Salinity = 0), k_w can be calculated as follows:

$$k_w = (0.333U_{10} + 0.222U_{10}^2)(Sc/600)^{-0.5} \tag{7}$$

where U_{10} is the wind speed at 10 m high and Sc is the Schmidt number which is the ratio between the diffusivity (Wise and Houghton, 1968) of CO and the kinematic viscosity (Korson et al., 1969; Millero, 1974) of seawater. The seawater temperature and salinity generated by a physical mixing model were used to calculate Sc.

2.1.3. Vertical mixing (V)

Due to sunlight attenuation through the water column, CO concentration should be higher at the sea surface, decreasing exponentially with depth assuming uniform CDOM distribution. However, vertical mixing may redistribute the dissolved CO molecules within the mixed layer. In a one-dimensional (1-D) context, the vertical mixing of [CO] within water column is described by:

$$V(z, t) = -\frac{\partial}{\partial z}\left\{(D_z + \varepsilon)\frac{\partial}{\partial z}[CO]\right\} \tag{8}$$

where D_z and ε are the eddy and molecular diffusivities, respectively. The turbulent fluxes in the marine boundary layer can be calculated by means of various different turbulence closure models, e.g., Kettle (2005). Here, we have used the k-ε turbulence closure scheme in the General Ocean Turbulence Model (GOTM, www.gotm.net) as previously done by Kettle (2005a) and Burchard and Petersen (1999).

2.1.4. A new formulation of microbial oxidation (M)

We assumed that microbial oxidation rate of CO (M) is better represented by a second-order decay function of CO concentration and bacterial biomass:

$$M = -k_{bio}[B][CO] \tag{9}$$

where k_{bio} is a new microbial oxidation rate coefficient and [B] is a bacterial biomass concentration in carbon unit. It is worthwhile to note that the k_{bio} multiplied by [B] is the same to the conventional k_{CO} (h^{-1}). Thus the unit of k_{bio} is same to k_{CO} divided by [B]. Since the spatial and the temporal variabilities of k_{CO} are implicitly represented by those of [B], the new coefficient k_{bio} can be assumed to be constant in any environment.

It should be noted that the CO oxidized by bacteria is converted in the model to dissolved inorganic carbon (DIC) since CO is used for energy and not for carbon assimilation (Jones and Amador, 1993; Moran and Miller, 2007; Tolli and Taylor, 2005).

2.2. Implementation of the coupled CO-GOTM-ERSEM model and set-up for BATS

The new formulation of microbial CO oxidation requires the explicitly simulated bacteria biomass. For this reason, we have embedded the proposed CO formulation in the European Regional Seas Ecosystem Model (ERSEM, Butenschön et al., 2016) which is one of the few marine ecosystem models that explicitly simulates bacterial biomass (Baretta-Bekker et al., 1995; Blackford et al., 2004; Butenschön et al., 2016; Polimene et al., 2006). ERSEM has been coupled with GOTM and implemented at BATS as previously done to simulate bulk pelagic ecosystem properties and DMS(P) dynamics (Butenschön et al., 2016; Polimene et al., 2012).

BATS is the only site where dissolved CO concentrations time-series were measured along with physical and biological parameters allowing to put CO dynamic in a wider ecosystem context.
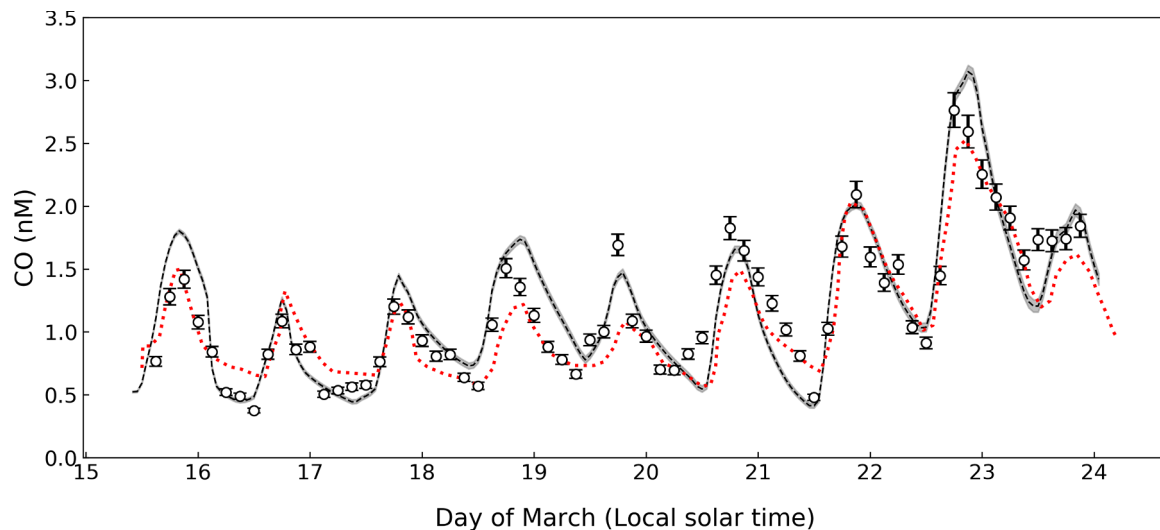
Fig. 2. Comparison of model simulations by Kettle (2005b) with the optimized source and sink terms and the dark production term (red dashed line), the present study (black dashed line) with shade for uncertainties by standard deviation of k_{bio}, and the observation (open circle, Kettle (1994)) of dissolved CO concentration. (For interpretation of the references to colour in this figure legend, the reader is referred to the web version of this article.)

Table 1
Statistical matrix of model performances in simulating surface CO concentrations by Kettle (2005b) and the present study. The optimization means multiplication of a proper constant to the CO source and sink terms to obtain the best simulating performance.

	Kettle, 2005b without optimization	Kettle, 2005b with optimization	This study
RMSE	0.4	0.3	0.3
R	0.9	0.9	0.9
MBE	0.0	− 0.1	0.0

Since the maximum mixed layer depth (MLD) at BATS was not deeper than 190 m during the year in 1993 (Steinberg et al., 2001), we confined the model depth to 210 meter consisting of 60 equidistant vertical layers. It is assumed that there is no upward flux across the model's bottom boundary, while the downward flux such as particle sinking is allowed. Model initial conditions and parameters were taken from Butenschön et al. (2016). Atmospheric forcing data were obtained from the European centre for Medium-Range Weather Forecast Reanalysis data product (ERA-Interim, Dee et al., 2011).

The model without the CO module was run for 30 years to get semi-steady state of ecosystem variables by assimilating the vertical profiles of temperature and salinity (T/S) observed at BATS constrained by the repeated atmospheric forcing in 1991. Since the interval of observed T/S profiles in 1991 varied between 1 and 3 months, the relaxation time scale of T/S was set at 30 days. The surface boundary conditions of the model were forced by 6-hourly meteorology in 1991. Using the final state of the 30-year spin-up as initial conditions, the model was further integrated until March 15, 1993 with 6-hourly corresponding ERA-interim forcing to generate the initial conditions for the ecosystem state variable used in the 9-day simulation described in the next section.

2.3. Nine-day simulation for the determination of optimum k_{bio}

Kettle (1994) measured the CO concentrations in the surface waters at BATS for 9 days in March 1993. These data have been used to test the new CO model and to estimate the value of k_{bio}.

To compensate for missing hydrodynamic impacts of lateral advection and diffusion, simulated T and S were relaxed toward observed profiles. For this short simulation we used the wind speed and irradiance observed by Kettle (1994) which offered a higher temporal

resolution (less than 1 min) with respect to ERA-Interim (6 h). A constant CO profile (equal to the mean value observed on 15th March 1993) was given as initial condition to allow the model to redistribute CO within the water column following its dynamics.

Bayesian optimization (Snoek et al., 2012) was employed to determine the most appropriate k_{bio} using the 9-day CO observations. With each iterative calculation of the objective function (Root-Mean-Square-Error (RMSE) of CO in this study) bounding the pre-specified ranges of k_{bio}, the algorithm updates the k_{bio} and incorporates the new k_{bio} into the next estimate of RMSE until it converges to minimum. Since the k_{CO} suggested by Kettle (2005b) divided by simulated bacteria biomass on 15 of March 1993 is order of 1E-03, we set the lower and upper limit for the search space of k_{bio} as $1E-04$ and $1E-02$ (mg C m^{-3})$^{-1}$ h^{-1}, respectively.

The uncertainty of k_{bio} was estimated by Monte-Carlo method by generating 100 sets of the dissolved CO concentrations in time-series that are randomly varied within 5% of the CO concentrations, which is the analytical uncertainty (Kettle, 1994). Mean and standard deviation of the 100 simulations were adopted as the optimal k_{bio} and its error, respectively.

To investigate how k_{bio} value responds to the source and sink terms of CO budget, sensitivity experiments were carried out with respect to the photochemical production (J), air-sea gas exchange (F), and vertical mixing (V) rates because they can be variable depending on the different parameterizations. Simulation without perturbation of $J, F,$ and V was assigned as 'control' simulation below. For the sensitivity runs, the $J, F,$ and V were individually perturbed by ± 20% and ± 10% of those of the control simulation. Sensitivity of k_{bio} for each term is defined as,

$$SN_l = \frac{\left(\frac{\Delta k_{bio}}{k_{bio}}\right)}{\left(\frac{\Delta T_l}{T_l}\right)} \tag{10}$$

where T_l denotes the budget term l of control run and ΔT_l the perturbed T_l. l is one of $J, F,$ and V and ΔT_l is one of $0.8T_l, 0.9T_l, 1.1T_l,$ and $1.2T_l$.

2.4. Multiyear simulation

To investigate seasonal to inter-annual variability of CO, 3-year simulation (from 1992 to 1994) was carried out. The bacterial biomasses observed for the same period at BATS as part of US Joint Global Ocean Flux Study (Steinberg et al., 2001) were used to validate the model simulation and to see how the variation of bacterial biomass impacts
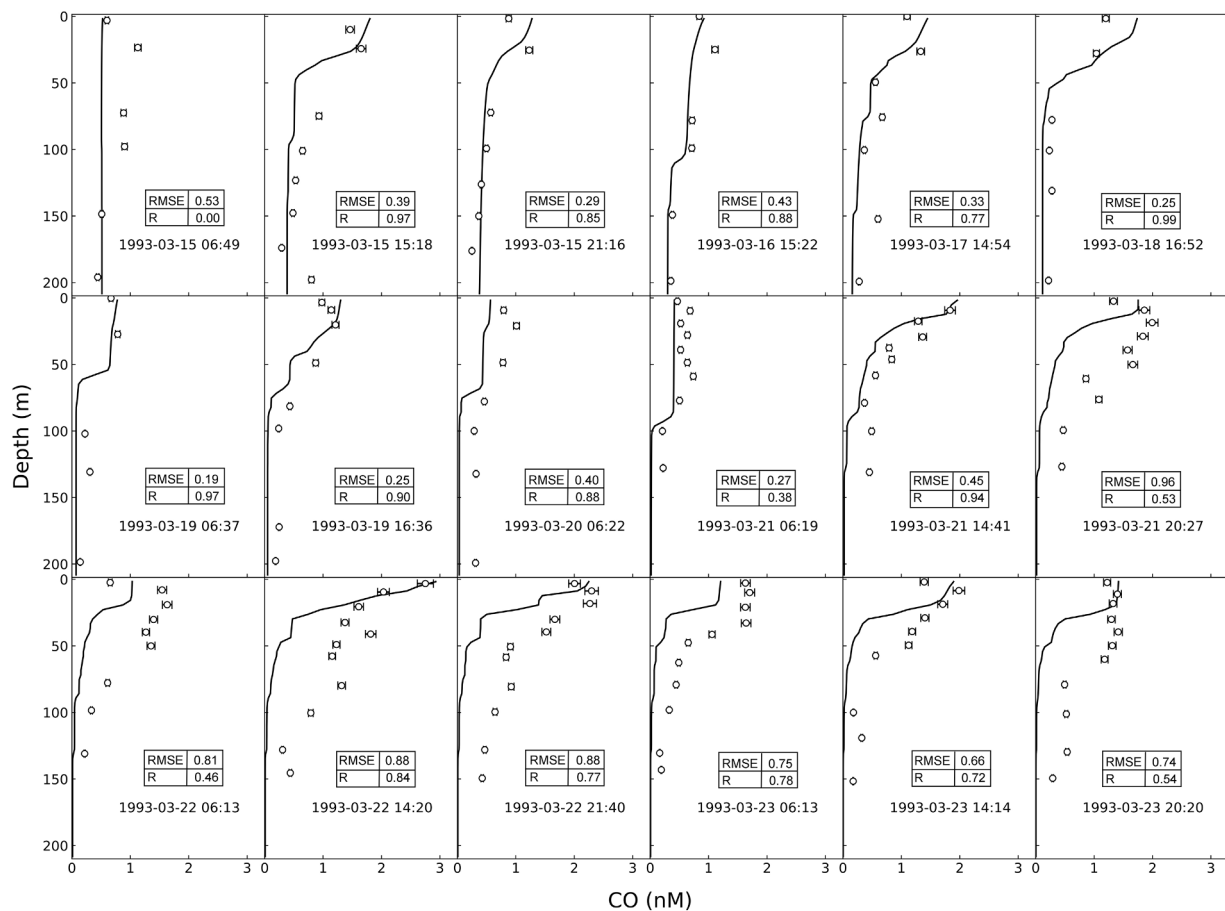
Fig. 3. Comparison of a time series of simulated (solid line) and measured (open circle; from Kettle (1994)) depth profiles of dissolved CO concentrations. Individual graphs include the time (local solar time) the profile was gained, and RMSE and Pearson coefficient, R. (For interpretation of the references to colour in this figure legend, the reader is referred to the web version of this article.)

the microbial oxidation. To this purpose, observed bacterial cell density (cells kg^{-1}) was converted to carbon mass unit by a conversion factor of 10 fg C cell^{-1} (Steinberg et al., 2001).

For this simulation we used the optimum k_{bio} determined in Section 2.3. CO-GOTM-ERSEM was restarted from the 30-year spin-up state of GOTM-ERSEM coupled model. The meteorology was forced by the 6-hourly ERA-interim data and the model T/S profiles were relaxed toward the observed profiles with the relaxation time scale of a month.

2.5. Model evaluation metrics

We used three quantitative metrics, root-mean-squared error (RMSE), mean-bias error (MBE), and Pearson correlation coefficient (R) to assess our CO model skill suggested by Jolliff et al. (2009). RMSE is defined as the square root of the variance between simulated and observed values, and MBE as the difference between the means of model and of observation fields. RMSE and MBE measure the degree of discrepancies between the model prediction and the observation. Thus, the closer their values are to zero, the better the model accuracy is. The Pearson correlation coefficient (R), defined here by the covariance of model and of observation fields divided by the product of their standard deviations, is a measure of the degree of linear association between model and observations. RMSE, MBE, and R give quantitative information particularly when evaluating the sensitivity of a model to a specific parameter to minimize the magnitude of fitness between model and observation (Jolliff et al., 2009).

3. Results

3.1. Nine-day simulation with optimum k_{bio}

The microbial oxidation rate coefficient, k_{bio}, in the new CO-GOTM-ERSEM model determined by the procedure described in Section 2.3 was 5.7 ± 0.2 (μg C m^{-3})$^{-1}$ h^{-1}. We present here the model performance focusing on the surface CO concentrations as well as their vertical distributions. Sensitivity results of the k_{bio} to the perturbations of CO sources and sinks are also presented.

3.1.1. Surface CO concentration

Simulated and observed (Kettle, 1994) surface CO concentrations during the 9 days from Mar. 15 to 24, 1993 are displayed in Fig. 2. The observed diel variations and the gradual increasing trend of surface CO concentrations are well reproduced by the model. The good performance of our new model was confirmed by a set of statistical metrics (RMSE, MBE, and R). As shown in Table 1, our model performs slightly better than a previously published model (Kettle, 2005b) regardless of applying the optimization technique. However, R values from both models are identical.

3.1.2. Vertical profiles of CO concentration

In Fig. 3, the simulated CO profiles are compared with the observations by Kettle (1994). Overall, the model underestimates the observed CO especially below the MLD where the simulated CO concentrations are close to zero while the observations never fall below 0.2 nM. However, the high correlation between simulated and observed
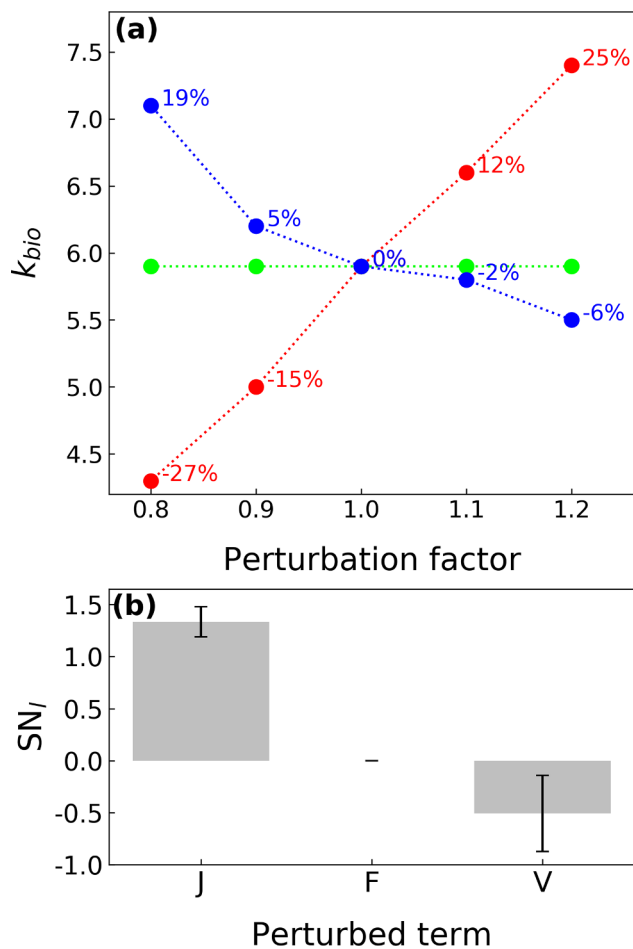
Fig. 5. Simulated (black) and observed (red) bacterial biomasses in the surface mixed layer from 1992 to 1994. (For interpretation of the references to colour in this figure legend, the reader is referred to the web version of this article.)

a^{-1} observed between 1992 and 1994. However, simulated bacterial biomass overestimates the observed values by 30% on average. While the vernal bloom of bacteria was captured by the model for 1992 and 1993, the low values observed in spring of 1994 were not reproduced in the simulations. If we exclude this period from the comparison, R and MBE values are 0.7 and 1.3, respectively, confirming the general good performance of the model.

3.2.2. Seasonal cycles of bacterial biomass and CO

The simulated seasonal cycles of bacterial biomass and surface CO concentration are illustrated in Fig. 6a. CO concentrations display low values (1 nM) in spring, concomitantly with high bacterial biomass. CO starts to increase by the onset of stratification due to radiative heating and by the reduction of bacterial biomass ($\sim$ 2.5 nM). From May to August, CO remains high (4 - 5 nM) with a peak concentration in July (mid-summer) driven by the combination of strong photochemical production, weak vertical mixing, and reduced bacterial biomass. From September (early fall) to January (winter), CO concentration declines to below 1 nM in association with the decrease of photochemical production, small increase of microbial oxidation, and deepened MLD. Since the CO oxidation is a function of bacterial biomass, its seasonality exactly follows bacterial biomass. The corresponding conventional oxidation rate coefficient (k_{CO}) shows its seasonal maximum in March and minimum in August.

The mean vertical distributions of CO and k_{CO} from the 3-year simulation are displayed in Fig. 6b. The highest k_{CO} appears at subsurface between 30 m and 50 m depth, just above the MLD. On the other hand, the simulated CO concentration maximum occurs at the surface because of the high irradiance and slightly lowered bacterial biomass.

4. Discussion

4.1. Meaning of the second-order loss kinetics

Microbial oxidation is the dominant sink of CO in seawater overwhelming air–sea gas exchange under normal turbulent conditions at the sea surface (Gnanadesikan, 1996; Zafiriou et al., 2003). It is therefore crucial to accurately parameterize this process if we want to simulate dissolved CO concentrations in a reliable way. In this work, we propose a new model including variable bacterial biomass in the formulation of CO oxidation. Our model is supported by literature findings showing that the conventional k_{CO} is not constant in the ocean. Indeed, k_{CO} is higher in the coastal areas than in the open ocean (Jones and Amador, 1993; Xie et al., 2005), in the subsurface layer than in the bottom and surface layers (Jones, 1991; Kettle, 1994; Kwon, 2015), and during phytoplankton bloom than during non-productive periods (Johnson and Bates, 1996; Jones and Amador, 1993; Zhang and Xie, 2012). All these studies suggest that it is unlikely that microbial oxidation of CO is only dependent on CO concentration as assumed in

Fig. 4. (a) Variation of optimized values of k_{bio} depending on the perturbation of J (red), V (blue), and F (lime) terms. Numbers on the line represent relative changes in k_{bio} with respect to the control run. (b) Sensitivities of k_{bio} (SN) to photoproduction (J), air-sea gas exchange (F), and vertical mixing (V). Error bars represent one standard deviation. (For interpretation of the references to colour in this figure legend, the reader is referred to the web version of this article.)

values (average R $\sim$ 0.8) indicates that the model captures the general trend of the observations as for example the depth where concentrations rapidly decrease. Nevertheless, the aforementioned underestimation of the observed values at depth reduces the overall performance of the model as highlighted by the relatively large RMSE values (mean RMSE = 0.53 $\pm$ 0.26).

3.1.3. Sensitivity of k_{bio} to CO source and sinks

Our experiments indicate that the air-sea gas exchange rate (F) has negligible effects on the determination of k_{bio}. Overall, k_{bio} is more sensitive to the photochemical production rate (J) than to the physical mixing rate (V) (Fig. 4). k_{bio} is inversely related to V because it acts as a sink by dilution of dissolved CO. As shown in Fig. 4b, the SN_J was calculated as 1.32, SN_F as 0, and SN_V as -0.5.

3.2. Multiyear simulation from 1992 to 1994

3.2.1. Bacterial biomass

The bacterial biomass measured at BATS varied between 3 and 8 mg C m^{-3} with a slight decreasing trend of 0.4 mg C m^{-3} a^{-1} (Fig. 5). The simulated bacterial biomass exhibits a clear seasonality with high values in spring and a gradual decrease toward fall and winter which is consistent with the observations (Steinberg et al., 2001). In addition, the model reproduced the gradual decreasing trend of 0.4 mg C m^{-3}
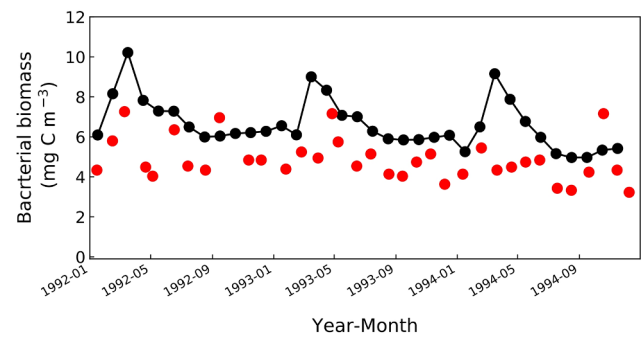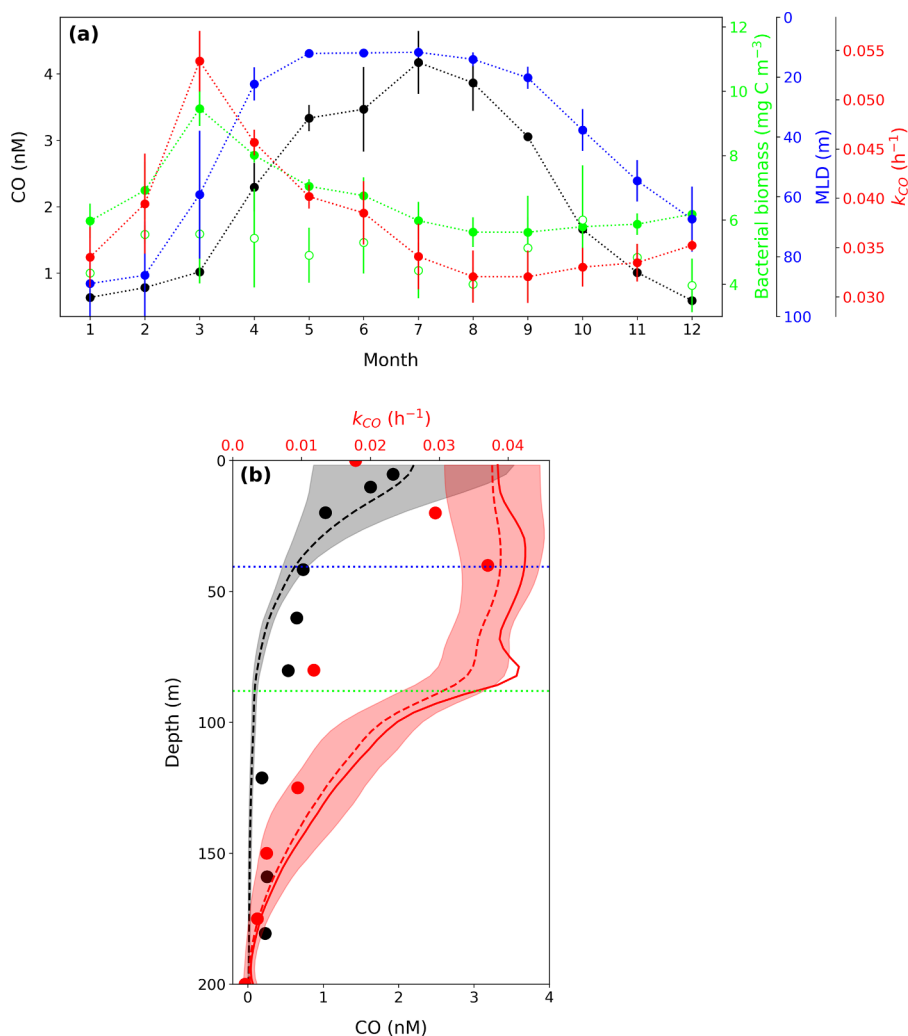
Fig. 6. (a) Monthly mean CO concentrations (black solid circle) and bacterial biomasses (lime solid circle) at the sea surface, and monthly mean MLDs (blue solid circle) for model simulation from 1992 to 1994. Red solid circles denote the monthly mean of CO oxidation rates (k_{CO}). Lime open circles indicate monthly mean values of bacterial biomass observed. Error bars represent one standard deviation. (b) Simulated vertical profiles of k_{CO} (red) and of CO concentrations (black). Broken lines represent their mean values simulated from 1992 to 1994 and shade for uncertainties (one standard deviation). Red solid line denotes the simulated mean profile of k_{CO} in June, and black and red closed circles for measured CO and k_{CO} in June 1987 by Jones (1991), respectively. Dotted horizontal lines denote the 3-year mean values of MLD (blue) and euphotic depth (yellow). (For interpretation of the references to colour in this figure legend, the reader is referred to the web version of this article.)

previously published models (Gnanadesikan, 1996; Kettle, 2005b; Kitidis et al., 2011; Conte et al., 2018). We argue that, like other microbial processes, the microbial CO oxidation is affected by microbial density and community composition, supply of organic and inorganic substrates, and other conditions such as temperature and pH (Rivkin and Anderson, 1997; Rivkin et al., 1996).

Our new model allows k_{CO} to vary spatially and temporally, reflecting the dependency of bacterial growth on environmental conditions and in this way connecting the marine CO cycle to broader ecosystem functions. The seasonal variability of CO in our model is consistent with the observations reported by Jones (1991) who described large CO variability in the Sargasso Sea between June of 1986 and September of 1987. Jones (1991) found that both CO concentration and k_{CO} in June were higher than in September (by 1.7 and 2 times, respectively). Another observed k_{CO} value at the Sargasso Sea in summer (Aug. 1999) was reported as 0.02 ± 0.002 h^{-1} (Tolli and Taylor, 2005), showing a similarity with our summer value ($\sim 0.03 \pm 0.003$ h^{-1}; Fig. 6a). Johnson and Bates (1996) explained the almost 4 times higher CO concentration observed in summer with respect to winter by the synergetic effect of high irradiance and lower oxidation rate due probably to low abundance of bacteria.

In addition to the temporal/seasonal variation, modelled k_{CO} also varies with depth following bacterial distribution (Fig. 6b). This is consistent with previous studies reporting that k_{CO} decreased gradually with depth reaching its maximum at about 40 m deep (Jones, 1991) and that bacterial biomass at BATS reaches its maximum between 30 and 80 meter depth (Steinberg et al., 2001).

Since primary production is likely to be affected by the global climate change (Cavan et al., 2019; Moore et al., 2018), further studies should be designed to assess how global-warming driven alterations of the planktonic ecosystem might affect the global CO budget and the role of CO as a climate change driver.

4.2. Critical assessment of model assumptions

Inclusion of bacterial biomass in the new parameterization of CO oxidation assumes that a constant fraction of the heterotrophic bacterial community is involved in CO oxidation. This assumption is supported by previous studies reporting that *Roseobacter*-associated clade cells responsible for the fastest CO metabolism are ubiquitous in marine environments accounting for 36 ± 2.4 % of the total microbial assemblage (Tolli et al., 2006). However, since Tolli et al. (2006) only considered samples from coastal waters, further studies are necessary to assess the validity of our assumption in wide range of marine environments.

Our model reproduced at least qualitatively the maximal bacterial biomass in the subsurface layers (Fig. 7c) and the consequent maximum of k_{CO} (Fig. 6b). However, the model significantly overestimates both bacterial biomass and k_{CO} below 40 m. Indeed, Steinberg et al. (2001) reported the bacterial biomass < 2.0 mg C m^{-3} at depths less than 150 m regardless of the season, while our model simulated circa 5 mg C m^{-3} at the same depth except for winter (Fig. 7c). Fig. 7 illustrates that bacterial biomass is coupled to dissolved organic carbon (DOC) reaching their maxima at $\sim$80 m near the subsurface Chl-*a* maximum
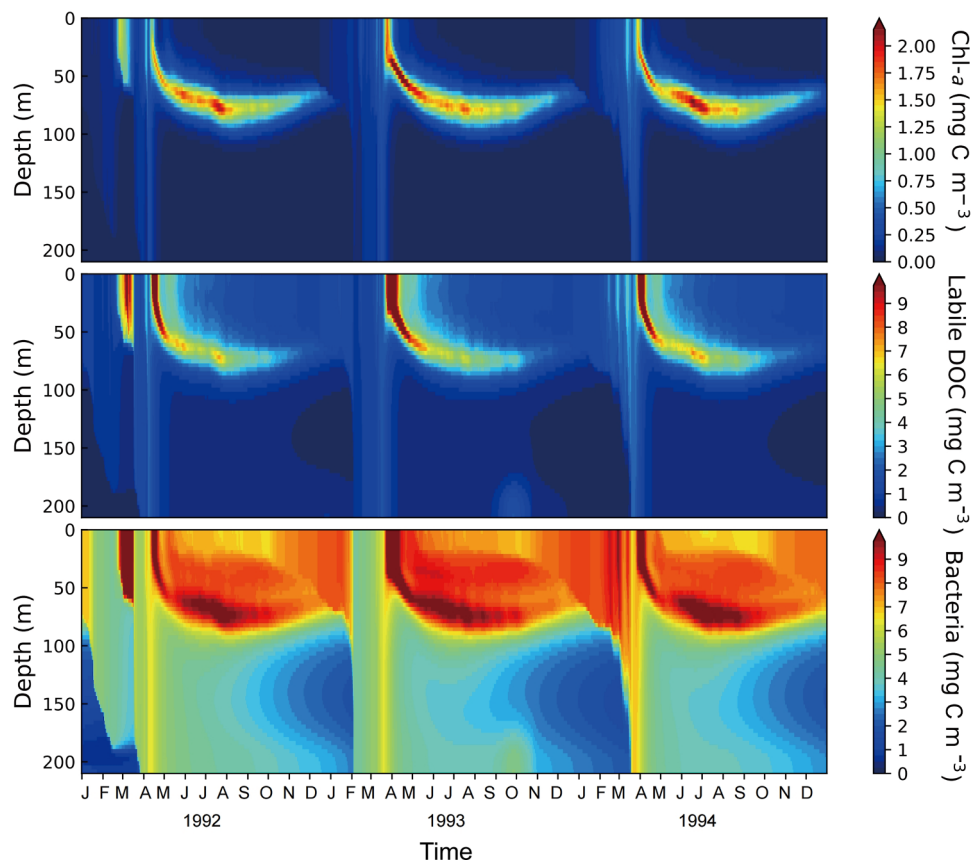
Fig. 7. Time-depth distribution of (a) Chl-*a*, (b) labile DOC concentration, and (c) bacterial biomass simulated for the 3-year (1992 - 1994) simulation at BATS.

(Steinberg et al., 2001). This is consistent with previous findings and theoretical modeling studies showing a correlation between phytoplankton (or Chl-*a*) and bacterial production, underlining the dependence of bacterial growth on a pool of DOC 'freshly' produced by the primary producers (Dumont et al., 2011; Wiebinga and de Baar, 1998; Polimene et al., 2006).

The overestimation of bacteria in the subsurface layer can be mainly explained by overestimation of DOC which is the main source of carbon and energy for heterotrophic bacteria. Since total organic carbon (TOC) observations in 1994 are available and it is dominated by DOC in BATS (Hansell and Carlson, 1998), we compared TOC rather than DOC (Fig. 8). The simulated TOC between 100 - 210 m depth was overestimated about 40%. Despite the overestimated bacterial biomass and DOC, our model reproduced a realistic relationship among primary production, DOC and bacteria. Indeed, the simulated DOC tends to concentrate at the subsurface layers since phytoplankton populates the subsurface layer to avoid nutrient-limited surface waters. The most salient feature of our model is to connect CO dynamics and primary production. This connection is established through bacterial abundance and distribution and DOC production and fate.

Another element to be considered is that we did not resolve the CDOM dynamics explicitly, assuming that the CDOM absorbance is constant. However, Siegel et al. (2002) observed non-homogeneous vertical distribution of CDOM absorbance at BATS with larger values observed at the depths between 50 and 100 m suggesting that the photochemical production of CO may differ depending on the depth. Given that the k_{bio} is highly sensitive to the change of photoproduction rate (Fig. 4), additional studies are required to shed light on CDOM absorbance variability and refine our model accordingly.
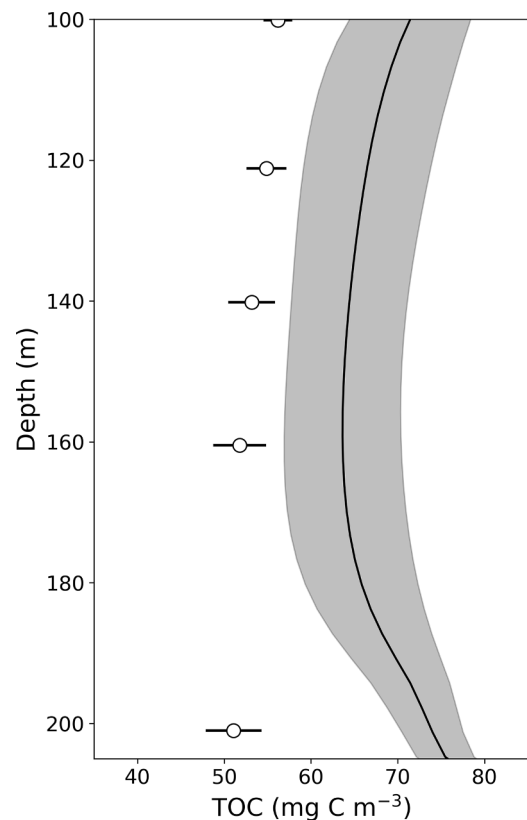

Fig. 8. Comparison of observed and simulated total organic carbon (TOC) during March to November of 1994 at BATS (Hansell and Carlson, 2001). Solid line and the shaded range denote simulated mean and standard deviation, respectively, and open circle the observations.

5. Conclusions

A CO model was developed with a new parameterization of microbial oxidation, the dominant sink of CO in the ocean. We suggested a new parameterization implying a second-order loss kinetics depending on bacterial biomass other than CO concentration. The new parameterization introduces a universal constant k_{bio} which describes the bacterial biomass specific CO oxidation rate. By optimizing CO simulations against the 9-day observations of surface CO concentrations at BATS (Kettle, 1994), k_{bio} was estimated to be 5.7 $\pm$ 0.2 $(\mu g\ C\ m^{-3})^{-1}$ h^{-1}. Using this k_{bio} value, our simulations carried out with CO-GOTM-ERSEM, reproduced the observed temporal (seasonal and inter-annual) and spatial (vertical) variability of CO oxidation rate and CO concentrations. Further studies assessing the dependency of CO on bacterial biomass and DOC would be required to evaluate if the k_{bio} derived in this study is applicable in other oceanic contexts.

Credit_Author_Statement

Young Shin Kwon: Conceptualization, Writing-Original draft preparation, Software, Data curation Visualization, Formal analysis, Funding acquisition

Hyoun-Woo Kang: Supervision, Methodology, Writing- Original draft preparation, Funding acquisition

Luca Polimene: Writing-Reviewing and Editing, Funding acquisition

Tae Siek Rhee: Writing-Reviewing and Editing, Supervision, Funding acquisition

Declaration of Competing Interest

The authors declare that they have no known competing financial interests or personal relationships that could have appeared to influence the work reported in this paper.

Acknowledgments, samples, and data

References

Anderson, N.J., Stedmon, C.A., 2007. The effect of concentration on dissolved organic carbon concentration and quality in lakes of SW Greenland. Freshwater Biol 52 (2), 280–289. https://doi.org/10.1111/j.1365-2427.2006.01688.x.

Asmala, E., Stedmon, C.A., Thomas, D.N., 2012. Linking CDOM spectral absorption to dissolved organic carbon concentrations and loadings in boreal estuaries. Estuar Coast Shelf Sci 111, 107–117. https://doi.org/10.1016/j.ecss.2012.06.015.

Baretta-Bekker, J.G., Baretta, J.W., Koch Rasnesseb, E., 1995. The microbial food web in the european regional seas ecosystem model. Netherlands journal of sea research 33, 363–379.

Bates, T.S., Kelly, K.C., Johnson, J.E., Gammon, R.H., 1995. Regional and seasonal-variations in the flux of oceanic carbon-monoxide to the atmosphere. Journal of Geophysical Research-Atmosphere 100 (D11), 23093–23101. https://doi.org/10.1029/95jd02737.

Blackford, J.C., Allen, J.I., Gilbert, F.J., 2004. Ecosystem dynamics at six contrasting sites: a generic modelling study. Journal of marine systems 52 (1–4), 191–215. https://doi.org/10.1016/j.jmarsys.2004.02.004.

Bricaud, A., Babin, M., Morel, A., Claustre, H., 1995. Variability in the chlorophyll-specific absorption-coefficients of natural phytoplankton - analysis and parameterization. Journal of Geophysical Research: Oceans 100 (C7), 13321–13332. https://doi.org/10.1029/95jc00463.

Bricaud, A., Morel, A., Prieur, L., 1981. Absorption by dissolved organic matter of the sea (yellow substance) in the UV and visible domains 1. Limnol. Oceanogr. 26 (1), 43–53.

Burchard, H., Petersen, O., 1999. Models of turbulence in the marine environment - a comparative study of two-equation turbulence models. Journal of marine systems 21 (1–4), 29–53. https://doi.org/10.1016/S0924-7963(99)00004-4.

Butenschön, M., Clark, J., Aldridge, J.N., Allen, J.I., Artioli, Y., Blackford, J., ... Lessin, G., 2016. ERSEM 15.06: a generic model for marine biogeochemistry and the ecosystem dynamics of the lower trophic levels. Geoscientific Model Development 9 (4), 1293–1339.

Cavan, E.L., Henson, S.A., Boyd, P.W., 2019. The Sensitivity of Subsurface Microbes to Ocean Warming Accentuates Future Declines in Particulate Carbon Export. Front Ecol Evol 6. https://doi.org/10.3389/fevo.2018.00230.

Coble, P.G., 2007. Marine optical biogeochemistry: the chemistry of ocean color. Chem. Rev. 107 (2), 402–418. https://doi.org/10.1021/cr050350.

Conrad, R., Seiler, W., Bunse, G., Giehl, H., 1982. Carbon monoxide in seawater (Atlantic Ocean). Journal of Geophysical Research: Oceans 87 (C11), 8839–8852.

Conte, L., Szopa, S., Séférian, R., Bopp, L., 2018. The oceanic cycle of carbon monoxide and its emissions to the atmosphere. Biogeosciences Discussions 1–33. https://doi.org/10.5194/bg-2018-410.

Daniel, J.S., Solomon, S., 1998. On the climate forcing of carbon monoxide. Journal of Geophysical Research: Atmosphere 103 (D11), 13249–13260. https://doi.org/10.1029/98jd00822.

Dee, D.P., Uppala, S.M., Simmons, A., Berrisford, P., Poli, P., Kobayashi, S., Andrae, U., Balmaseda, M., Balsamo, G., Bauer, d.P., 2011. The ERA-Interim reanalysis: configuration and performance of the data assimilation system. Quarterly Journal of the royal meteorological society 137 (656), 553–597.

Doney, S.C., Najjar, R.G., Stewart, S., 1995. Photochemistry, mixing and diurnal cycles in the upper ocean. J. Mar. Res. 53 (3), 341–369. https://doi.org/10.1357/0022240953213133.

Dumont, I., Schoemann, V., Jacquet, S.H.M., Masson, F., Becquevort, S., 2011. Bacterial abundance and production in epipelagic and mesopelagic waters in the Subantarctic and Polar Front zones south of Tasmania. Deep Sea Research Part II: Topical Studies in Oceanography 58 (21–22), 2212–2221. https://doi.org/10.1016/j.dsr2.2011.05.024.

Ferrari, G.M., 2000. The relationship between chromophoric dissolved organic matter and dissolved organic carbon in the European Atlantic coastal area and in the West Mediterranean Sea (Gulf of Lions). Mar Chem 70 (4), 339–357. https://doi.org/10.1016/S0304-4203(00)00036-0.

Ferrari, G.M., Dowell, M.D., Grossi, S., Targa, C., 1996. Relationship between the optical properties of chromophoric dissolved organic matter and total concentration of dissolved organic carbon in the southern Baltic Sea region. Mar Chem 55 (3–4), 299–316. https://doi.org/10.1016/S0304-4203(96)00061-8.

Gibson, J., 2003. UVB radiation: definition and characteristics. USDA/CSU website. [Online.].

Gnanadesikan, A., 1996. Modeling the diurnal cycle of carbon monoxide: sensitivity to physics, chemistry, biology, and optics. Journal of Geophysical Research: Oceans 101 (C5), 12177–12191. https://doi.org/10.1029/96jc00463.

Gonzalez, J.M., Moran, M.A., 1997. Numerical dominance of a group of marine bacteria in the alpha-subclass of the class Proteobacteria in coastal seawater. Appl. Environ. Microbiol. 63 (11), 4237–4242.

Gonzalez, J.M., Simo, R., Massana, R., Covert, J.S., Casamayor, E.O., Pedros-Alio, C., Moran, M.A., 2000. Bacterial community structure associated with a dimethylsulfoniopropionate-producing North Atlantic algal bloom. Appl. Environ. Microbiol. 66 (10), 4237–4246.

Green, S.A., Blough, N.V., 1994. Optical-Absorption & Fluorescence Properties of Chromophoric Dissolved Organic-Matter in Natural-Waters. Limnol. Oceanogr. 39 (8), 1903–1916. https://doi.org/10.4319/lo.1994.39.8.1903.

Hansell, D.A., Carlson, C.A., 1998. Net community production of dissolved organic carbon. Global Biogeochem Cycles 12 (3), 443–453. https://doi.org/10.1029/98gb01928.

Hansell, D.A., Carlson, C.A., 2001. Biogeochemistry of total organic carbon and nitrogen in the Sargasso Sea: control by convective overturn. Deep Sea Research Part II: Topical Studies in Oceanography 48 (8–9), 1649–1667.

Ho, D.T., Wanninkhof, R., Schlosser, P., Ullman, D.S., Hebert, D., Sullivan, K.F., 2011. Toward a universal relationship between wind speed and gas exchange: gas transfer velocities measured with3He/SF6during the Southern Ocean Gas Exchange Experiment. J. Geophys. Res. 116. https://doi.org/10.1029/2010jc006854.

Johnson, J.E., Bates, T.S., 1996. Sources and sinks of carbon monoxide in the mixed layer of the tropical South Pacific Ocean. Global Biogeochem Cycles 10 (2), 347–359. https://doi.org/10.1029/96 gb00366.

Johnson, J.E., 1999. Evaluation of a seawater equilibrator for shipboard analysis of dissolved oceanic trace gases. Anal. Chim. Acta 395 (1–2), 119–132. https://doi.org/10.1016/S0003-2670(99)00361-X.

Jolliff, J.K., Kindle, J.C., Shulman, I., Penta, B., Friedrichs, M.A.M., Helber, R., Arnone, R.A., 2009. Summary diagrams for coupled hydrodynamic-ecosystem model skill assessment. Journal of Marine Systems 76 (1–2), 64–82. https://doi.org/10.1016/j.jmarsys.2008.05.014.

Jones, R.D., 1991. Carbon-Monoxide and Methane Distribution and Consumption in the Photic Zone of the Sargasso Sea. Deep-Sea Research 38 (6), 625–635. https://doi.org/10.1016/0198-0149(91)90002-W.

Jones, R.D., Amador, J.A., 1993. Methane and Carbon-Monoxide Production, Oxidation, and Turnover Times in the Caribbean Sea as Influenced by the Orinoco River. Journal of Geophysical Research: Oceans 98 (C2), 2353–2359. https://doi.org/10.1029/92jc02769.

Jones, R.D., Morita, R.Y., 1984. Effect of several nitrification inhibitors on carbon monoxide and methane oxidation by ammonium oxidizers. Can. J. Microbiol. 30 (10), 1276–1279.

Kettle, A.J., 1994. A Model of the Temporal and Spatial Distribution of Carbon Monoxide in the Mixed layer. Massachusetts institute of technology, Massachusetts, USA.

Kettle, A.J., 2000. Extrapolation of the Oceanic Flux of DMS, CO, COS, and CS$_2$. York University, Toronto, Ont., Canada.

Kettle, A.J., 2005a. Comparison of the nonlocal transport characteristics of a series of one-dimensional oceanic boundary layer models. Ocean Modelling 8 (4), 301–336. https://doi.org/10.1016/j.ocemod.2004.01.002.

Kettle, A.J., 2005b. Diurnal cycling of carbon monoxide (CO) in the upper ocean near Bermuda. Ocean Modelling 8 (4), 337–367. https://doi.org/10.1016/j.ocemod.2004.01.003.

Khalil, M.A.K., Rasmussen, R.A., 1990. The Global Cycle of Carbon-Monoxide - Trends and Mass Balance. Chemosphere 20 (1–2), 227–242. https://doi.org/10.1016/0045-6535(90)90098-E.

Kitidis, V., Tilstone, G.H., Smyth, T.J., Torres, R., Law, C.S., 2011. Carbon monoxide emission from a Mauritanian upwelling filament. Mar Chem 127 (1–4), 123–133. https://doi.org/10.1016/j.marchem.2011.08.004.

Korson, L., Drost-Hansen, W., Millero, F.J., 1969. Viscosity of water at various temperatures. J Phys Chem 73 (1), 34–39.

Kwon, Y.S., 2015. Contrasting Marine Carbon Monoxide Cycles in the North Pacific and the Amundsen Sea. University of Science and Technology, Daejeon, Korea.

Logan, J.A., Prather, M.J., Wofsy, S.C., McElroy, M.B., 1981. Tropospheric chemistry: a global perspective. Journal of Geophysical Research: Oceans 86 (C8), 7210–7254.

Mannino, A., Russ, M.E., Hooker, S.B., 2008. Algorithm development and validation for satellite-derived distributions of DOC and CDOM in the U.S. Middle Atlantic Bight. J. Geophys. Res. 113 (C7). https://doi.org/10.1029/2007jc004493.

Moore, J.K., Fu, W., Primeau, F., Britten, G.L., Lindsay, K., Long, M., Doney, S.C., Mahowald, N., Hoffman, F., Randerson, J.T., 2018. Sustained climate warming drives declining marine biological productivity. Science 359 (6380), 1139–1143. https://doi.org/10.1126/science.aao6379.

Millero, F.J., 1974. The physical chemistry of seawater. Annu Rev Earth Planet Sci 2 (1), 101–150.

Moran, M.A., Buchan, A., Gonzalez, J.M., Heidelberg, J.F., Whitman, W.B., Kiene, R.P., Henriksen, J.R., King, G.M., Belas, R., Fuqua, C., et al., 2004. Genome sequence of Silicibacter pomeroyi reveals adaptations to the marine environment. Nature 432 (7019), 910–913. https://doi.org/10.1038/nature03170.

Moran, M.A., Miller, W.L., 2007. Resourceful heterotrophs make the most of light in the coastal ocean. Nature Reviews Microbiology 5 (10), 792–800. https://doi.org/10.1038/nrmicro1746.

Nelson, N.B., Siegel, D.A., 2013. The global distribution and dynamics of chromophoric dissolved organic matter. Annu Rev Earth Planet Sci 5, 447–476. https://doi.org/10.1146/annurev-marine-120710-100751.

Nelson, N.B., Siegel, D.A., Michaels, A.F., 1998. Seasonal dynamics of colored dissolved material in the Sargasso Sea. Deep-Sea Research Part I 45 (6), 931–957. https://doi.org/10.1016/S0967-0637(97)00106-4.

Nightingale, P.D., Malin, G., Law, C.S., Watson, A.J., Liss, P.S., Liddicoat, M.I., Boutin, J., Upstill-Goddard, R.C., 2000. In situ evaluation of air-sea gas exchange parameterizations using novel conservative and volatile tracers. Global Biogeochem Cycles 14 (1), 373–387. https://doi.org/10.1029/1999 gb900091.

Park, K., Rhee, T.S., 2016. Oceanic source strength of carbon monoxide on the basis of basin-wide observations in the Atlantic. Environmental Science Processes & Impacts 18 (1), 104–114. https://doi.org/10.1039/c5em00546a.

Polimene, L., Allen, J.I., Zavatarelli, M., 2006. Model of interactions between dissolved organic carbon and bacteria in marine systems. Aquatic microbial ecology 43 (2), 127–138. https://doi.org/10.3354/ame043127.

Polimene, L., Archer, S.D., Butenschön, M., Allen, J.I., 2012. A mechanistic explanation of the Sargasso Sea DMS "summer paradox". Biogeochemistry 110 (1–3), 243–255. https://doi.org/10.1007/s10533-011-9674-z.

Price, J.F., Weller, R.A., Pinkel, R., 1986. Diurnal cycling - observations and models of the upper ocean response to diurnal heating, cooling, and wind mixing. Journal of Geophysical Research: Oceans 91 (C7), 8411–8427. https://doi.org/10.1029/JC091iC07p08411.

Redden, G.D., 1982. Characteristics of Photochemical Production of Carbon Monoxide in Seawater. Oregon State University.

Rhee, T.S., 2000. The Process of Air-Water Gas Exchange and Its Application. Texas A&M University College Station, Texas, USA.

Rivkin, R.B., Anderson, M.R., 1997. Inorganic nutrient limitation of oceanic bacterioplankton. Limnol. Oceanogr. 42 (4), 730–740.

Rivkin, R.B., Anderson, R., Lajzerowicz, C., 1996. Microbial processes in cold oceans. I. Relationship between temperature and bacterial growth rate. Aquatic microbial ecology 10, 243–254.

Rochelle-Newall, E.J., Fisher, T.R., 2002. Chromophoric dissolved organic matter and dissolved organic carbon in Chesapeake Bay. Mar Chem 77 (1), 23–41. https://doi.org/10.1016/S0304-4203(01)00073-1.

Siegel, D.A., Maritorena, S., Nelson, N.B., Hansell, D.A., Lorenzi-Kayser, M., 2002. Global distribution and dynamics of colored dissolved and detrital organic materials. Journal of Geophysical Research: Oceans 107 (C12). https://doi.org/10.1029/2001JC000965. 21-21-21-14.

Sikorski, R.J., Zika, R.G., 1993. Modeling mixed-layer photochemistry of H$_2$O$_2$ - optical and chemical modeling of production. Journal of Geophysical Research: Oceans 98 (C2), 2315–2328. https://doi.org/10.1029/92jc02933.

Snoek, J., Larochelle, H., Adams, R.P., 2012. Practical bayesian optimization of machine learning algorithms. Adv Neural Inf Process Syst 25, 2951–2959.

Stedmon, C.A., Markager, S., Kaas, H., 2000. Optical properties and signatures of chromophoric dissolved organic matter (CDOM) in Danish coastal waters. Estuar Coast Shelf Sci 51 (2), 267–278. https://doi.org/10.1006/ecss.2000.0645.

Steinberg, D.K., Carlson, C.A., Bates, N.R., Johnson, R.J., Michaels, A.F., Knap, A.H., 2001. Overview of the US JGOFS Bermuda Atlantic Time-series Study (BATS): a decade-scale look at ocean biology and biogeochemistry. Deep-Sea Research Part II 48 (8–9), 1405–1447. https://doi.org/10.1016/S0967-0645(00)00148-X.

Stocker, T.F., Qin, D., Plattner, G.-.K., Tignor, M., Allen, S.K., Boschung, J., Nauels, A., Xia, Y., Bex, V., Midgley, P.M., 2013. Climate Change 2013: The physical Science basis, Edited. Cambridge University Press, Cambridge.

Stubbins, A., Uhera, G., Kitidis, V., Law, C.S., Upstill-Goddard, R.C., Woodward, E.M.S., 2006. The open-ocean source of atmospheric carbon monoxide. Deep-Sea Research Part II 53 (14–16), 1685–1694. https://doi.org/10.1016/j.dsr2.2006.05.010.

Suzuki, M.T., Beja, O., Taylor, L.T., Delong, E.F., 2001. Phylogenetic analysis of ribosomal RNA operons from uncultivated coastal marine bacterioplankton. Environ. Microbiol. 3 (5), 323–331.

Tolli, J.D., Sievert, S.M., Taylor, C.D., 2006. Unexpected diversity of bacteria capable of carbon monoxide oxidation in a coastal marine environment, and contribution of the Roseobacter-associated clade to total CO oxidation. Appl. Environ. Microbiol. 72 (3), 1966–1973. https://doi.org/10.1128/AEM.72.3.1966-1973.2006.

Tolli, J.D., Taylor, C.D., 2005. Biological CO oxidation in the Sargasso Sea and in Vineyard Sound, Massachusetts. Limnol. Oceanogr. 50 (4), 1205–1212. https://doi.org/10.4319/lo.2005.50.4.1205.

Valentine, R.L., Zepp, R.G., 1993. Formation of carbon monoxide from the photodegradation of terrestrial dissolved organic carbon in natural waters. Environ. Sci. Technol. 27 (2), 409–412.

Vodacek, A., Blough, N.V., DeGrandpre, M.D., Peltzer, E.T., Nelson, R.K., 1997. Seasonal variation of CDOM and DOC in the Middle Atlantic Bight: terrestrial inputs and photooxidation. Limnol. Oceanogr. 42 (4), 674–686. https://doi.org/10.4319/lo.1997.42.4.0674.

Wanninkhof, R., 2014. Relationship between wind speed and gas exchange over the ocean revisited. Limnology and Oceanography: Methods 12 (6), 351–362. https://doi.org/10.4319/lom.2014.12.351.

Wiebinga, C.J., de Baar, H.J.W., 1998. Determination of the distribution of dissolved organic carbon in the Indian sector of the Southern Ocean. Mar Chem 61 (3–4), 185–201. https://doi.org/10.1016/s0304-4203(98)00014-0.

Wiesenburg, D.A., Guinasso, N.L., 1979. Equilibrium solubilities of methane, carbon monoxide, and hydrogen in water and sea water. Journal of Chemical & Engineering Data 24 (4), 356–360. https://doi.org/10.1021/je60083a006.

Wise, D., Houghton, L., 1968. Diffusion coefficients of neon, krypton, xenon, carbon monoxide and nitric oxide in water at 10–60 C. Chem Eng Sci 23 (10), 1211–1216.

Xie, H.X., Belanger, S., Demers, S., Vincent, W.F., Papakyriakou, T.N., 2009. Photobiogeochemical cycling of carbon monoxide in the southeastern Beaufort Sea in spring and autumn. Limnol. Oceanogr. 54 (1), 234–249. https://doi.org/10.4319/lo.2009.54.1.0234.

Xie, H.X., Zafiriou, O.C., Umile, T.P., Kieber, D.J., 2005. Biological consumption of carbon monoxide in Delaware Bay, NW Atlantic and Beaufort Sea. Mar. Ecol. Prog. Ser. 290, 1–14. https://doi.org/10.3354/meps290001.

Zafiriou, O.C., Joussot-Dubien, J., Zepp, R.G., Zika, R.G., 1984. Photochemistry of natural waters. Environ. Sci. Technol. 18 (12) 358A-371A.

Zafiriou, O.C., Andrews, S.S., Wang, W., 2003. Concordant estimates of oceanic carbon monoxide source and sink processes in the Pacific yield a balanced global "bluewater" CO budget. Global Biogeochem Cycles 17 (1). https://doi.org/10.1029/2001gb001638.

Zhang, Y., Xie, H.X., 2012. The sources and sinks of carbon monoxide in the St. Lawrence estuarine system. Deep-Sea Research Part II 81-84, 114–123. https://doi.org/10.1016/j.dsr2.2011.09.003.

Zuo, Y.G., Jones, R.D., 1995. Formation of carbon-monoxide by photolysis of dissolved marine organic material and its significance in the carbon cycling of the oceans. Naturwissenschaften 82 (10), 472–474. https://doi.org/10.1007/Bf01131598.